Biophysical Journal Volume 69 October 1995 1334–1343

Transbilayer Pores Formed by β-Barrels: Molecular Modeling of Pore Structures and Properties

M. S. P. Sansom and I. D. Kerr
Laboratory of Molecular Biophysics, The Rex Richards Building, University of Oxford, Oxford OX1 3QU, United Kingdom

ABSTRACT Transmembrane β-barrels, first observed in bacterial porins, are possible models for a number of membrane channels. Restrained molecular dynamics simulations based on idealized Cαβ templates have been used to generate models of such β-barrels. Model β-barrels have been analyzed in terms of their conformational, energetic, and pore properties. Model β-barrels formed by $N = 4$, 8, 12 and 16 anti-parallel Ala_{10} strands have been developed. For each N, β-barrels with shear numbers $S = N$ to $2N$ have been modeled. In all β-barrel models the constituent β-strands adopt a pronounced right-handed twist. Interstrand interactions are of approximately equal stability for all models with $N \geq 8$, whereas such interactions are weaker for the $N = 4$ β-barrels. In $N = 4$ β-barrels the pore is too narrow (minimum radius ~0.6 Å) to allow ion permeation. For $N \geq 8$, the pore radius depends on both N and S; for a given value of N an increase in S from N to $2N$ is predicted to result in an approximately threefold increase in pore conductance. Calculated maximal conductances for the β-barrel models are compared with experimental values for porins and for K^+ channels.

INTRODUCTION

At first it was assumed that all integral membrane proteins, including ion channels and transport proteins, were formed by bundles of transmembrane (TM) α-helices. More recently, it has become evident that TM β-barrels also may form transbilayer pores. The best characterized such β-barrels occur in the bacterial porins (Jap and Walian, 1990), for which five crystallographic structures are known. In four cases the transbilayer pore is formed by a 16-stranded anti-parallel β-barrel (Cowan et al., 1992; Weiss and Schulz, 1992; Kreusch and Schulz, 1994); in maltoporin the β-barrel contains 18 strands (Schirmer et al., 1995). As well as the bacterial porins, β-barrels are believed to occur in mitochondrial (Benz, 1994) and plant plastid (Fischer et al., 1994) porins, although the precise topology of these barrels remains uncertain. More recently, transbilayer pores lined by β-barrels have been suggested to occur in K^+ and related voltage-gated channels (Bogusz et al., 1992; Durell and Guy, 1992; Bradley and Richards, 1994); epithelial Na^+ channels (Guy and Durell, 1995); aquaporin (Fischbarg et al., 1995); and pores formed by the bacterial toxin aerolysin (Parker et al., 1994).

An interest in the TM β-barrel as a pore-forming protein motif is of particular significance in the context of structure prediction of membrane transport proteins. Several studies have explored prediction of β-barrel topologies on the basis of sequence analysis (Jeanteur et al., 1991; Fischbarg et al., 1993). To extend such studies to tertiary structure predictions an understanding of structural principles will be required. In the more general context of β-barrels in globular proteins (Lasters et al., 1988; Chothia and Murzin, 1994), important theoretical insights have been generated by the work of, among others, Murzin et al. (1994a,b). These authors analyzed the geometrical properties of idealized β-barrels in terms of the number of strands (N) and of the shear number (S, a measure of the stagger of the strands within a β-sheet). Considerations of permitted strand geometry and of optimal packing of side chains within a barrel suggested that only 10 different combinations of N and S should occur. However, it was noted that those β-barrels with central pockets or pores need not fall into these 10 combinations. Thus, pore-forming β-barrels may differ somewhat from β-barrels in general.

In this paper we extend theoretical structural investigations to idealized pores formed by anti-parallel β-barrels. Simple hydrophobic β-barrels with a range of combinations of N and S are modeled via restrained molecular dynamics (MD) simulations, using a simulated annealing protocol similar to that employed in our previous studies of TM α-helix bundles (Kerr et al., 1994; Breed et al., 1995; Sansom et al., 1995). The geometry and energetics of the resultant β-barrels are analyzed. Pore radius profiles are calculated and used to estimate the maximum ionic conductance possible for a given (N, S) combination. Finally, comparisons are made with the β-barrel structures observed experimentally in bacterial porins, and with those proposed as models of voltage-gated and other K^+ channels.

MATERIALS AND METHODS

Programs

MD simulations and model building were carried out using Xplor V3.1 (Brünger, 1992) with the CHARMM PARAM19 (Brooks et al., 1983) parameter set. Only those H atoms attached to polar groups were represented explicitly, apolar groups being represented using extended atoms. Display and examination of models was carried out using Quanta V4.0 (Molecular Simulations, Waltham, MA), and structure diagrams drawn

Received for publication 28 April 1995 and in final form 3 July 1995.

Address reprint requests to Dr. Mark S. P. Sansom, Laboratory of Molecular Biophysics, University of Oxford, The Rex Richards Building, South Parks Road, Oxford OX1 3QU U.K. Tel.: 44-1865-275371; Fax: 44-1865-510454; E-mail: mark@biop.ox.ac.uk.

0006-3495/95/10/1334/10 $2.00

using Molscript (Kraulis, 1991). MD simulations were performed on a DEC 3000 400 computer. All other calculations were carried out on a Silicon Graphics Indy workstation.

Cαβ template geometry

Our restrained MD simulations require as input a Cαβ template. This is an initial model of a β-barrel structure in which approximate positions are specified for the Cα and Cβ atoms. The remainder of the structure is generated automatically during simulated annealing (see below). Idealized β-barrels for use as Cαβ templates were constructed using the parameters defined by Murzin et al. (1994a). Thus, N is the number of anti-parallel β-strands, and S is the shear number, defined as follows. If one starts at residue 1 in strand 1 and moves around the barrel in a direction perpendicular to the strands until one returns to strand 1, then because of the stagger between the strands one returns not to residue 1 but to residue S-1. Thus S is a measure of the extent of stagger of the strands; the greater the value of S the greater the stagger, and thus the greater the tilt of the strand axes relative to the pore axis. If one considers a flattened β-sheet (see Fig. 2, *A–C* for an example) of N strands with a shear number S, then the grid defining the Cα atom positions within such a sheet is determined by three parameters: a = the Cα-Cα distance along the strands; b = the interstrand distance; and α = the angle of the strands relative to the barrel (z) axis. Following Murzin et al. (1994a) we used a = 3.3 Å and b = 4.4 Å, with the slope of the strands given by:

$$\alpha = \tan^{-1}\left[\frac{S}{N} \cdot \frac{a}{b}\right].$$

Having generated a flat sheet of Cα atoms, this is then "rolled up" to form a β-barrel of radius

$$R = \frac{b}{[2\sin(\pi/N)\cos\alpha]}.$$

Cβ atoms were added to alternating sides of each strand by positioning them ±1.5 Å along radial vectors to the corresponding Cα atom. The resultant template was then used to generate an all atom model of a barrel by restrained MD simulated annealing.

Simulated annealing

The simulated annealing protocol used was similar to that already described in the context of modeling bundles of TM helices (Kerr et al., 1994; Sansom et al., 1995), and so only details specific to the current study are described. Backbone atoms other than Cα were superimposed on the Cα atoms of the corresponding residues. The Cα atoms of the strands remained fixed throughout stage 1, while all other atoms were unrestrained. Annealing started at 1000 K, during which weights for covalent terms were gradually increased. A repulsive van der Waals potential was slowly introduced after an initial delay. Once the weights for these terms reached their final values, the system was cooled from 1000 to 300 K in steps of 10 K and 0.5 ps. During cooling, van der Waals radii were reduced to 80% of their standard values in order to enable atoms to pass by one another. Electrostatic terms were not included during stage 1.

Structures from stage 1 were each subjected to five MD runs (stage 2), resulting in an ensemble of five final structures. Initial velocities were assigned corresponding to 500 K. Harmonic restraints were imposed on Cα atoms of the helices at the beginning of stage 2, and were gradually relaxed as the temperature was reduced from 500 to 300 K. Backbone torsion angle restraints were also introduced at this point (see below). On reaching 300 K, a 5 ps burst of constant temperature dynamics was performed, followed by 1000 steps of conjugate gradient energy minimization. During the latter burst of dynamics and energy minimization no positional restraints were imposed on the Cα atoms, but torsion angle restraints were maintained. During stage 2 electrostatic interactions were introduced into the potential energy function. All atoms are assigned partial charges as defined by the PARAM19 parameter set, and a distance-dependent dielectric ($\epsilon = r$) was used. A cutoff of 9 Å was used in evaluating non-bonded interactions, both van der Waals and electrostatic, and this cutoff was smoothed using a switch function.

To maintain strand geometry during simulated annealing, backbone torsion angle restraints were imposed. These were imposed using the Xplor dihedral angle restraint function:

$$E = C(\chi - \chi_{LOW})^2 \quad \text{if} \quad \chi < \chi_{LOW}$$

$$E = 0 \quad \text{if} \quad \chi_{LOW} < \chi < \chi_{HIGH}$$

$$E = C(\chi - \chi_{HIGH})^2 \quad \text{if} \quad \chi_{HIGH} < \chi$$

with C = 4.0 kcal/mol/rad^2. Thus, for β-strand geometry $\phi_{LOW} = -169°$, $\phi_{HIGH} = -109°$, and $\psi_{LOW} = +105°$, $\psi_{HIGH} = +165°$. These restraints correspond to a broad region centered about (ϕ, ψ) = (−139°, +135°) (Creighton, 1993). Interstrand H-bonds were not maintained explicitly.

Analysis

Variation within an ensemble of structures was determined via calculation of the main-chain atom RMSD. The overall conformation of β-strands within the barrels was analyzed in terms of the twist angle defined by, e.g., Chou et al. (1982a,b) as the pseudo-dihedral angle $\delta = O_i\text{-}C_i\text{-}C_{i+2}\text{-}O_{i+2}$.

The total potential energy of each structure (E_{TOT}) was evaluated, along with its van der Waals (E_{VDW}) and electrostatic (E_{ES}) components. Also evaluated was the strand-strand interaction energy, defined as $\Delta E = E$ (barrel) − E (isolated strands).

Pore radius profiles were measured using HOLE (Smart et al., 1993), which generates a pore radius (r) as a function of distance along the pore (z) axis. Thus, r_{MIN} is defined as the minimum of the pore radius profile. The length (l) of a pore is defined as the separation on z of the most extreme Cα atoms.

Pore radius profiles were used to estimate the maximum possible ionic conductance for a barrel. This was obtained by treating the pore as a cylinder of radius $r(z)$ (given by HOLE) of electrolyte of resistivity ρ. If pore runs from $z = a$ to $z = b$, then its overall electrical resistance is given by $R = R_a + R_{PORE} + R_b$, where R_a and R_b are the access resistances at either mouth of the pore (Hille, 1992) and where R_{PORE} is the resistance of the pore per se, obtained by integrating $\rho/(\pi r^2)$ along the length of the pore (Kuyucak and Chung, 1994). Thus, the maximum possible conductance is given by the reciprocal of R, i.e.,

$$G_{MAX} = \left[\frac{\rho}{4r_a} + \int_a^b \frac{\rho}{\pi r^2}\,dz + \frac{\rho}{4r_b}\right]^{-1}.$$

Values of G_{MAX} were calculated using ρ = 0.13 Ω. equivalent to the resistivity of 0.5 M KCl.

RESULTS

Models investigated

To identify those β-barrel geometries compatible with a transbilayer pore, a range of (N, S) combinations have been explored. Murzin et al. (1994a,b) demonstrated that optimal β-strand geometry requires a shear number within the range $S = N$ to $S = 2N$, and so models have been restricted to this range. The smallest β-barrel investigated was N = 4, as *a priori* it seemed likely that this could form a barrel but not a pore. At the other end of the scale an 18-strand barrel was

modeled, corresponding to that found in maltoporin. For each value of N, several values of S have been investigated. To summarize, models have been generated for 1) $N = 4$, $S = 4$, 6, and 8; 2) $N = 8$, $S = 8$, 12, and 16; 3) $N = 12$, $S = 12$, 16, 20 and 24; 4) $N = 16$, $S = 16$, 20 (as in four bacterial porins), 24, 28, and 32; and 5) $N = 18$, $S = 22$ (as in maltoporin).

So as to focus on underlying structural principles rather than on specific side-chain interactions, barrels have been modeled as anti-parallel Ac-Ala_{10}-NH_2 β-strands, i.e., simple hydrophobic β-strands. A 10-residue β-strand has a length of ~33 Å, which should be compared with an average thickness for the hydrocarbon core of a bilayer of ~30 Å (White, 1994). Furthermore, in the four $N = 16$ bacterial porins, the mean β-strand length is ~11 residues. Interstrand loop lengths are quite variable within the porins, and some of the loops are folded back into the lumen of the pore. In order to focus on the β-barrel architecture per se, interstrand loops were omitted from the models. Instead, each β-strand started with an N-acetyl group and ended with a C-terminal amide to mimic the presence of preceding and following peptide bonds within a pore-forming integral membrane protein.

The simulated annealing procedure yields an ensemble of structures. Preliminary calculations revealed that variation within an ensemble was somewhat less for β-barrels than in earlier studies of TM α-helix bundles (Kerr et al., 1994; Sansom et al., 1995) and so ensembles of five structures were judged to be sufficient to represent each N, S combination. Variation within an ensemble ($N = 8$, $S = 12$) is illustrated in Fig. 1. Superposition of the Cα traces reveals that there is some variation in backbone conformations, particularly at the termini of the β-strands. However, statistical analysis (see below) reveals that variation within ensembles is less than that between different (N, S) ensembles, confirming that a sample of five structures is sufficiently large to reveal underlying structural patterns.

The effect of varying the shear number, S, is illustrated for $N = 8$ β-barrels in Fig. 2. The increase in the tilt angle (α) of the β-strands consequent upon increasing S is evident from the diagrams of Fig. 2, *A–C*. Thus, for $S = 8$, 12, and 16, $\alpha = 37°$, 48° and 56°, respectively. The shapes of the corresponding β-barrels are shown in the ribbon diagrams in Fig. 2, *D–F*. Overall, for a given value of N, increasing S from N to $2N$ switches from a longer and narrower pore to a shorter and wider pore.

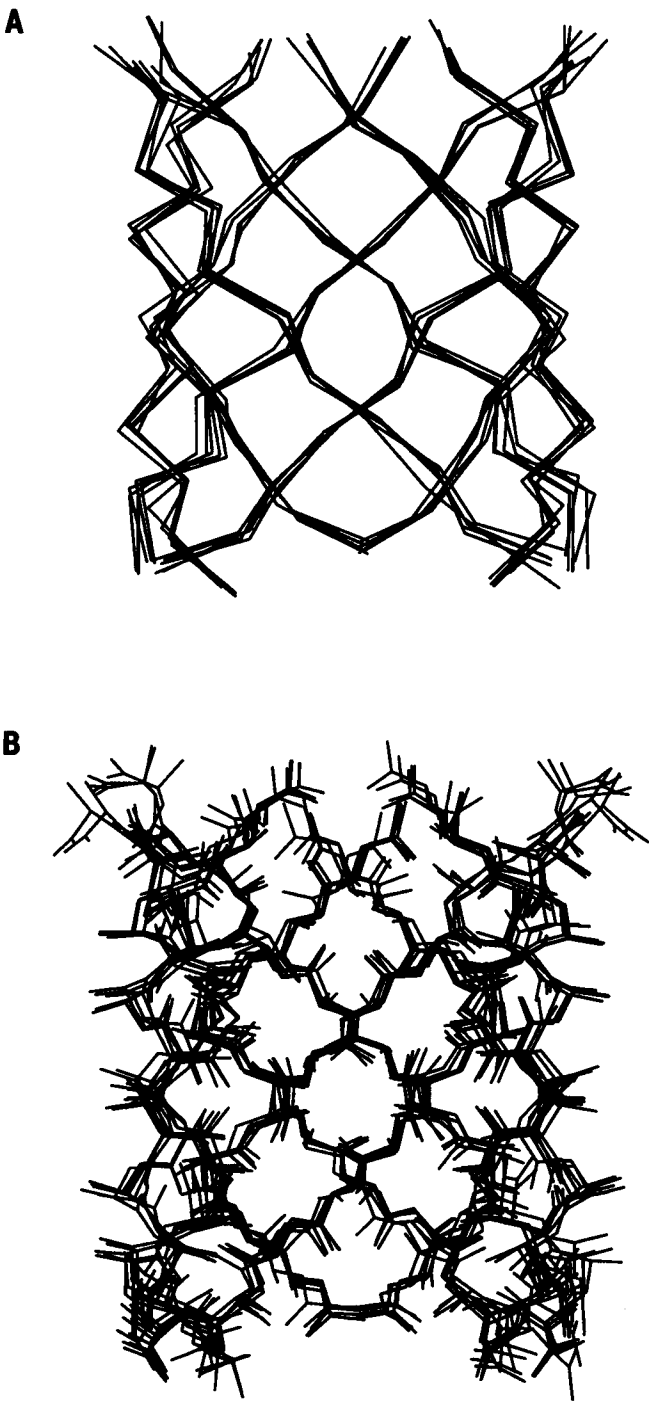

FIGURE 1 An ensemble of five structures for the $N = 8$, $S = 12$ β-barrel model, viewed perpendicular to the pore (z) axis. *A* shows Cα traces; *B* shows all non-H atoms.

β-Strand conformation

Statistical analysis of the backbone conformations of the β-barrels is provided in Table 1, in which parameters are averaged across all members of an ensemble. This analysis confirms that variation within an ensemble is relatively low, corresponding to a backbone RMSD of the order of 0.5 Å. Two trends in the β-strand twist angles (δ) may be seen. 1) As N increases, δ decreases from $\delta \approx 40°$ for $N = 4$ to $\delta \approx 15°$ for $N = 18$. 2) For higher N barrels, as S increases, δ increases slightly. Positive values of δ, corresponding to a right-handed twist of the β-strands, are observed in β-sheets in globular proteins (Chothia et al., 1981) and also in the results of conformational energy calculations on Ala_N and on Val_N and Ile_N β-strands and β-sheets (Chou et al., 1982a,b, 1983; Chou and Scheraga, 1982). A decrease in

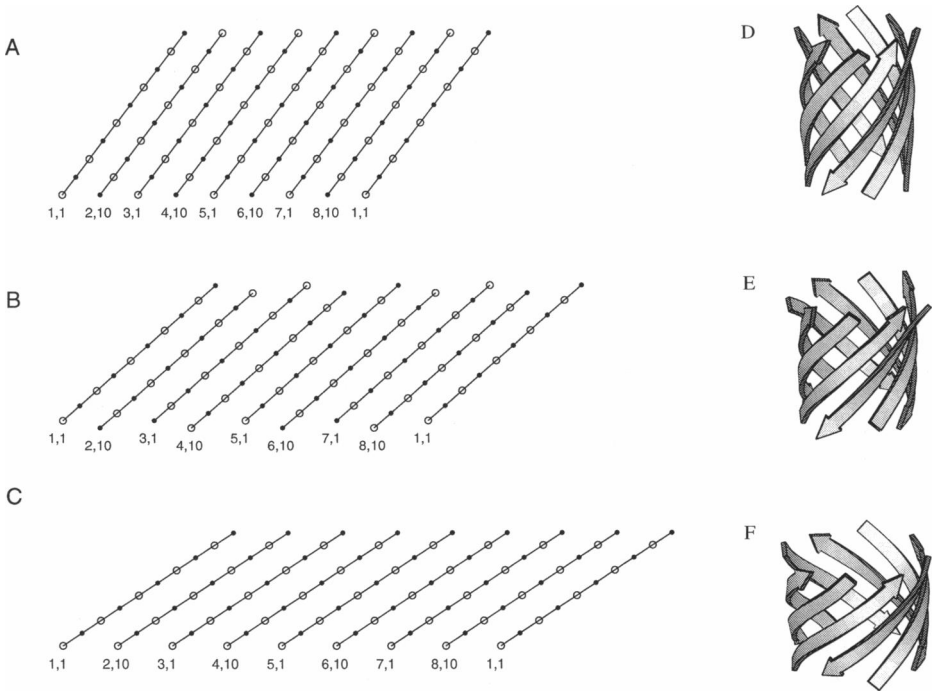

FIGURE 2 Effect of shear number (S) on β-barrel geometry. (*A–C*) Schematic diagrams of the β-sheets in $N = 8$, S = 8, 12, and 16 models, chosen at random from their respective ensembles. The diagrams correspond to β-barrels cut along strand β1 and unrolled. Strand β1 is shown twice, once on the left side and once on the right side. (○) Cα atoms whose Cβ atoms are above the page; (●) Cα atoms whose Cβ atoms are below the page. (*D–F*) Ribbon diagrams for the same three models (N = 8, S = 8, 12, and 16, respectively).

β-strand twist as N is increased was shown by Murzin et al. (1994a) in their theoretical study of β-barrels.

In addition to trends in δ as a function of N, S, changes in backbone (ϕ, ψ) angles are observed (Fig. 3). Thus, for a given value of N, as S increases ϕ increases and ψ decreases. This is evident in Ramachandran plots for the three $N = 8$ ensembles (Fig. 3); as S increases, (ϕ,ψ) values cluster around $\phi = -90°$, $\phi = +110°$. This lies to the right of the $\phi + \psi = 0$ line and so corresponds to a right-handed β-strand twist [i.e., $\delta > 0$; (Richardson and Richardson, 1989)]. Thus the trend in (ϕ,ψ) corresponds to that in δ, indicating an increase in the twist of the β-strands as S increases. This trend in Ramachandran plots was observed for all $N \geq 8$.

The pattern of H-bonding in the final structures was analyzed by visual inspection (using Quanta). In all structures H-bonding between adjacent strands of the barrel was close to the optimum expected for a given value of (N, S). Occasional deviations for the ideal pattern of interstrand H-bonding were observed at the termini of the strands, associated with local deviations of the termini from ideal β-strand conformation.

Overall, analysis of conformational statistics confirms that the simulated annealing procedure successfully converts ideal Cαβ templates to realistic β-barrels whose β-strand geometries are comparable with those observed in theoretical and experimental studies of β-sheet structures.

β-Barrel energetics

Potential energy statistics for the β-barrel ensembles are presented in Table 2. Such statistics reveal that for a given number of strands, N, the influence of the shear number, S, on the energetics of the barrels is complex. For $N \geq 8$, increasing S results in a decrease in E_{TOT}. This is the result of two opposing trends. 1) As S increases, E_{ES} increases as a result of an increase in the number of unsatisfied H-bonds between strands (see Fig. 2, *A–C*). 2) As S increases, E_{VDW} decreases. Thus, increasing the shear number, by increasing the strand twist angle, results in more favorable van der Waals interactions, but this effect is outweighed by loss of H-bonds between strands. As a consequence of this, for $N \geq 8$, either the $S = N$ or the $S = N + 4$ barrel is the most stable.

Pore properties

How may one assess the relevance of such radically simplified β-barrel models to an understanding transport and channel proteins? Pore radius profiles may be related to considerations of size exclusion of solutes by pores. Likewise, calculations of maximum pore conductances enable one to compare model β-barrels with experimentally determined ion channel properties. Statistics on pore dimensions and maximum conductance are given in Table 3.

From these data it is evident that $N = 4$ β-barrels form pores that are too narrow to support unhindered diffusion of ions. Thus, even for $N = 4$, $S = 8$, the β-barrel has a minimum pore radius of $r_{MIN} = 0.6$ Å, i.e., less than the ionic radius of a K^+ or Na^+ ion. On this basis it seems unlikely that $N = 4$ β-barrels can form the structural basis of ion channels. However, inspection of the pore radius profiles of $N = 4$ β-barrels (e.g., $N = 4$, $S = 8$ in Fig. 4 *A*)

TABLE 1 β-Barrel models: conformation

Models		RMSD			
N	S	(Å)	ϕ (°)	ψ (°)	δ (°)
4	4	0.56	−113 (±18)	+133 (±28)	+44 (±12)
4	6	0.84	−108 (±31)	+135 (±22)	+44 (±20)
4	8	0.57	−105 (±21)	+130 (±23)	+43 (±20)
8	8	0.38	−129 (±18)	+142 (±18)	+26 (±13)
8	12	0.53	−105 (±20)	+119 (±22)	+29 (±19)
8	16	0.48	−97 (±16)	+110 (±17)	+26 (±13)
12	12	0.69	−127 (±24)	+137 (±31)	+19 (±31)
12	16	0.53	−109 (±23)	+118 (±23)	+21 (±22)
12	20	0.51	−106 (±22)	+115 (±21)	+21 (±22)
12	24	0.71	−107 (±22)	+114 (±42)	+27 (±35)
16	16	0.57	−123 (±25)	+131 (±25)	+15 (±28)
16	20	0.60	−115 (±25)	+122 (±24)	+16 (±25)
16	24	0.57	−116 (±25)	+123 (±24)	+16 (±28)
16	28	0.53	−112 (±24)	+119 (±23)	+17 (±24)
16	32	0.61	−114 (±23)	+122 (±23)	+17 (±26)
18	22	0.63	−121 (±26)	+126 (±31)	+15 (±28)

reveals that for most of the length of the pore $r \approx 1$ Å. Conceivably, small changes in the local conformation of the barrel could be coupled to ion transport. Thus, $N = 4$ barrels should not be completely excluded from consideration as possible structures for transport proteins in general, even though they seem unlikely to occur in ion channels.

For $N \geq 8$, all the β-barrel models posses open pores. Inspection of pore radius profiles (Fig. 4) shows that r is approximately constant along the length of the pore. Thus, β-barrel pores do not exhibit pronounced "rings" of constrictions such as those seen in pores formed by bundles of parallel Ala_{20} and other α-helices (Kerr et al., 1994). The minimum pore radii of β-barrel models vary by a factor of 4.2 from smallest to largest; correspondingly the maximum conductances vary by a factor of 18.6 (i.e., $\approx 4.2^2$). For a given value of N, the pore radius increases by ~1.5× and the pore length decreases by ~1.5× as S is increased from $S = N$ to $S = 2N$. These two factors together contribute to a ~3-fold increase in G_{MAX}. That the major influence of N, S on conductance is via changes in pore radius and length was confirmed by calculations on simple equivalent cylinder models (data not shown). Thus, S is just as important as N in determining the pore properties (see Fig. 4). An extreme case of this is provided by comparison of the $N = 12$, $S = 24$ and $N = 16$, $S = 16$ pores; the latter exhibits a smaller conductance, despite having a larger number of β-strands within its barrel.

Comparisons with porins and K^+ channels

It is informative to compare the properties of model β-barrels with those observed experimentally for $N = 16$ bacte-

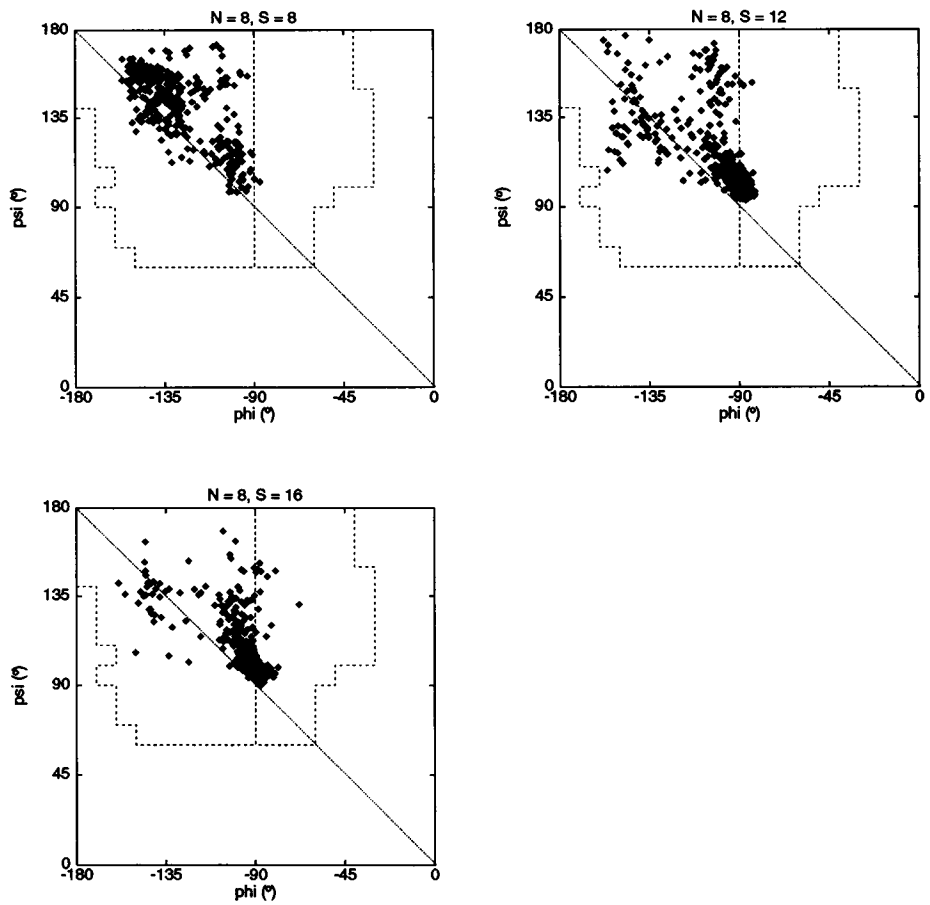

FIGURE 3 Ramachandran plots (upper left quadrant only) of (ϕ,ψ) values for the $N = 8$, S = 8 (*A*), $S = 12$ (*B*), and $S = 16$ (*C*) ensembles. The broken lines indicate the β_E and β_P regions as defined by Wilmot and Thornton (1990). The diagonal lines correspond to $\phi + \psi = 0$. Points to the right of this line correspond to a right-handed ($\delta > 0$) β-strand twist (Richardson and Richardson, 1989).

TABLE 2 β-Barrel models: energetics

Models		E_{TOT}	E_{VDW}	E_{ES}	$\Delta E_{TOT}/N$	$\Delta E_{VDW}/N$	$\Delta E_{ES}/N$
N	S	(kcal/mol)	(kcal/mol)	(kcal/mol)	(kcal/mol)	(kcal/mol)	(kcal/mol)
4	4	−652 (±5)	−118 (±2)	−593 (±6)	−61 (±1.0)	−19 (±0.5)	−42 (±1.3)
4	6	−656 (±5)	−125 (±5)	−603 (±8)	−65 (±4.3)	−22 (±1.5)	−42 (±3.5)
4	8	−667 (±4)	−129 (±5)	−614 (±4)	−67 (±2.3)	−22 (±0.5)	−45 (±1.5)
8	8	−1463 (±2)	−227 (±5)	−1331 (±6)	−77 (±0.3)	−20 (±0.3)	−57 (±0.3)
8	12	−1450 (±8)	−256 (±7)	−1287 (±5)	−75 (±0.3)	−22 (±0.9)	−52 (±1.0)
8	16	−1435 (±10)	−262 (±8)	−1262 (±5)	−70 (±0.5)	−23 (±0.8)	−47 (±0.3)
12	12	−2187 (±17)	−336 (±12)	−1975 (±21)	−76 (±1.2)	−20 (±0.4)	−56 (±1.0)
12	16	−2207 (±11)	−373 (±8)	−1950 (±6)	−76 (±0.3)	−22 (±0.6)	−54 (±0.6)
12	20	−2183 (±7)	−375 (±8)	−1923 (92)	−74 (±0.2)	−22 (±0.2)	−52 (±0.6)
12	24	−2123 (±6)	−370 (±6)	−1881 (±7)	−70 (±0.7)	−22 (±0.4)	−49 (±1.0)
16	16	−2957 (±6)	−457 (±3)	−2651 (±5)	−79 (±0.1)	−21 (±0.2)	−58 (±0.2)
16	20	−2936 (±9)	−476 (±14)	−2611 (±11)	−77 (±0.2)	−21 (±0.4)	−56 (±0.5)
16	24	−2902 (±7)	−469 (±10)	−2585 (±8)	−75 (±0.6)	−21 (±0.3)	−55 (±0.8)
16	28	−2888 (±8)	−478 (±10)	−2561 (±5)	−74 (±0.5)	−21 (±0.3)	−53 (±0.6)
16	32	−2864 (±6)	−469 (±11)	−2563 (±9)	−74 (±0.4)	−20 (±0.4)	−53 (±0.6)
18	22	−3295 (±20)	−525 (±9)	−2942 (±15)	−77 (±0.8)	−21 (±0.3)	−56 (±0.9)

E_{TOT}, total potential energy; E_{VDW}, van der Waals energy; E_{ES}, electrostatic energy; ΔE, strand–strand interaction energy.

rial porins and for K^+ channels. Fig. 5, *A* and *B* depicts the Cα traces of 1) *Rhodobacter capsulatus* porin (2POR; Weiss and Schulz, 1992); and 2) a structure from the $N = 16$, $S = 20$ ensemble. There are evident overall similarities between the model β-barrel and the porin structure, e.g., both exhibit a similar tilt of the β-strands relative to the barrel axis. However, the 2POR barrel is distorted from the ideal, being somewhat elliptical in cross-section. Also, there is a small difference in mean (ϕ,ψ) values for the pore residues: (−139°,+149°) for 2POR, (−115°, +122°) for the model. Thus the β-barrel models should be viewed as ideal structures that are subsequently modulated by e.g., the packing of interstrand loops.

The radius of the 2POR pore is considerably reduced by the L3 interstrand loop, which is folded down into the lumen of the pore. This is evident if one compares the pore radius profiles of 2POR and of the β-barrel model (Fig. 5 *C*). The profile for 2POR is less regular in shape and has a minimum pore radius of $r_{MIN} \approx 4.5$ Å, compared with $r_{MIN} = 10.4$ Å for the $N = 16$, $S = 20$ model. Thus, the β-barrel models enable us to calculate an upper limit on the size of solutes which could enter through a pore with a given N, S combination. However, this size limit may be considerably reduced by the presence on large interstrand loops within the pore lumen.

TABLE 3 β-Barrel models: pore properties

Models		r_{MIN}	l	G_{MAX}
N	S	(Å)	(Å)	(nS)
4	4		32	
4	6	0.6	28	0.07
4	8	0.6	23	0.09
8	8	2.9	32	0.71
8	12	3.5	27	1.2
8	16	4.8	21	2.4
12	12	6.1	31	2.5
12	16	6.8	28	3.3
12	20	8.2	25	4.9
12	24	9.8	23	6.6
16	16	9.5	32	5.1
16	20	10.4	32	6.1
16	24	11.8	28	7.9
16	28	13.3	25	10
16	32	15.1	22	13
18	22	12.3	30	7.9

G_{MAX} was calculated using $\rho = 0.13$ Ω (i.e., equivalent to 0.5 M KCl).

For the simple barrels G_{MAX} versus N (Fig. 6) exhibits a "band" of conductances for different S values, such that the "bandwidth" increases as N increases. Thus the β-barrel architecture per se allows considerable variation in conductance. One may usefully compare G_{MAX} values calculated from β-barrel models with calculated and experimentally determined values for $N = 16$ bacterial porins. From Fig. 6 it can be seen that the G_{MAX} values in 0.5 M KCl calculated on the basis of the four $N = 16$ porin x-ray structures cluster around 2 nS. This is significantly less than the value of $G_{MAX} = 6$ nS for a $N = 16$, $S = 20$ β-barrel model. Thus, a major effect of the L3 interstrand loop folded into the lumen of the porins is to reduce their maximum conductance by ~3-fold. However, the observed single channel conductance for the porins is still lower. For example, OmpF and PhoE (1OMF and 1PHO, respectively) have single channel conductances in 1 M NaCl of 0.8 nS and 0.6 nS, respectively (Cowan et al., 1992). Using calculated resistivities for 1 M NaCl and 0.5 M KCl these correspond to ~0.5 and 0.4 nS in 0.5 M KCl. Thus, the experimental single channel conductances are ~5-fold lower than the G_{MAX} values calculated on the basis of the crystallographic structures. One cause for this difference may be the nature of water within the pore. It has been shown for gramicidin A that water molecules exhibit altered dynamics within a channel (Chiu et al., 1991, 1993). MD simulations based on $N = 8$ β-barrel models (J. Breed, R. Sankararamakrishnan, I. D. Kerr, and M. S. P. Sansom,

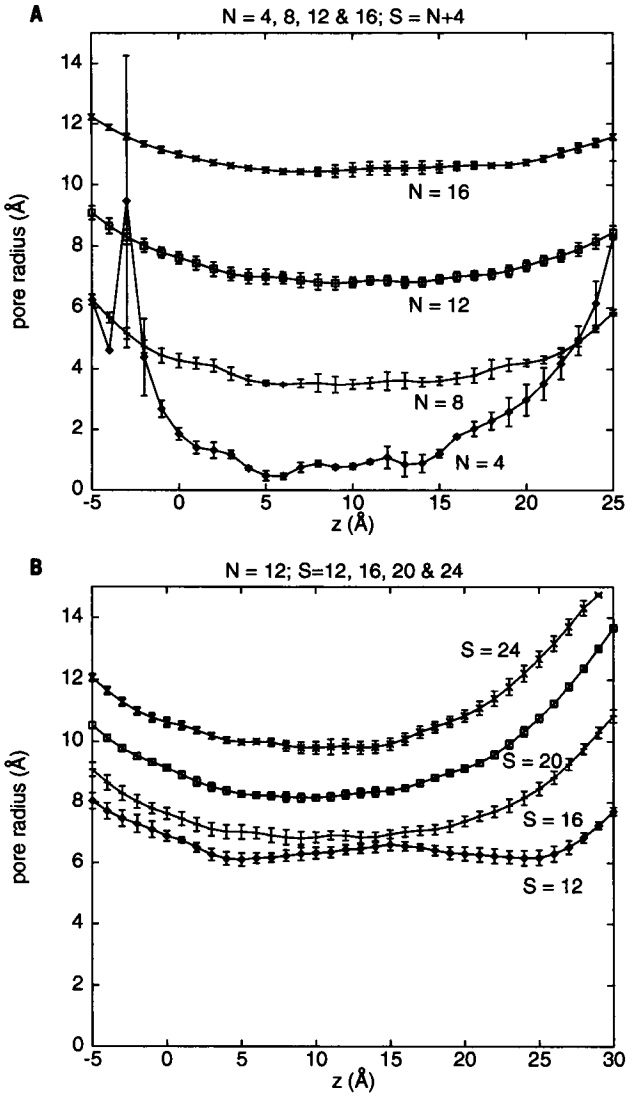

FIGURE 4 Pore radius profiles. Each profile is the ensemble average with error bars corresponding to ±SD. *A* shows profiles of $S = N + 4$ β-barrels for $N = 4$ (◇), $N = 8$ (+), $N = 12$ (□), and $N = 16$ (×). *B* shows profiles of $N = 12$ β-barrels for $S = 12$ (◇), $S = 16$ (+), $S = 20$ (□), and $S = 24$ (×).

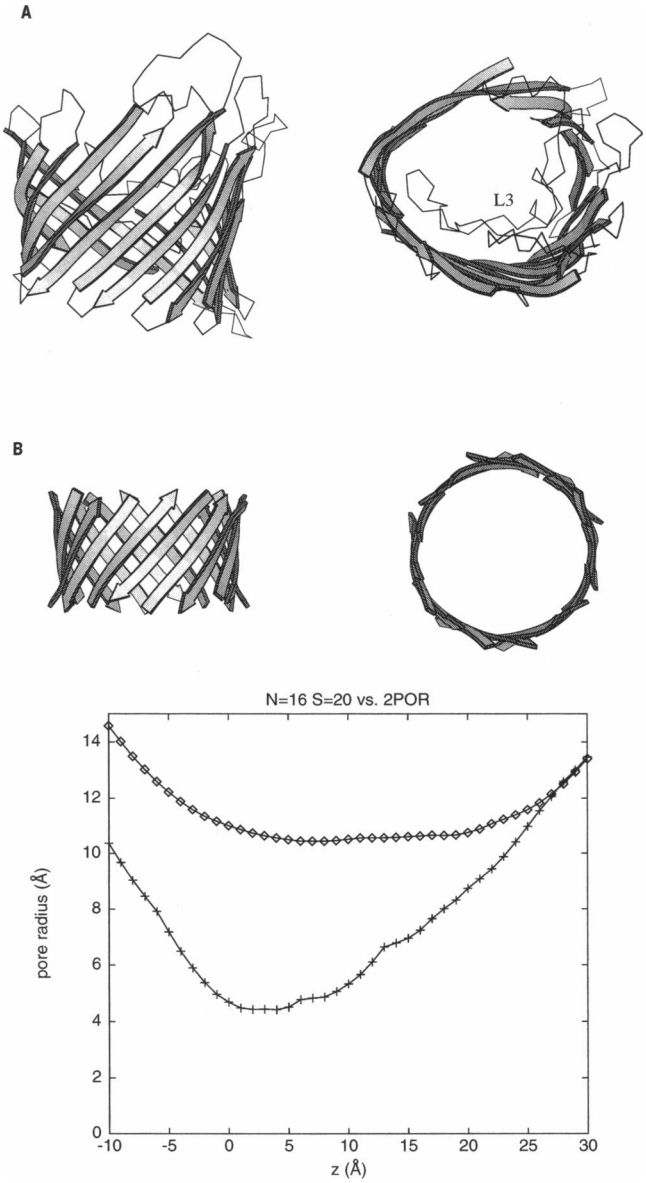

FIGURE 5 Comparison of (*A*) *R. capsulatus* porin (2POR) and (*B*) $N = 16$, $S = 20$ β-barrel Cα traces. β-strands are shown as arrows. Loop L3 is marked in the right view of 2POR. (*C*) Comparison of the pore radius profiles for 2POR and the $N = 16$, $S = 20$ ensemble. For 2POR $z = -10$ Å corresponds to the outer face of the β-barrel, and $z = +30$ Å to the periplasmic face. The constriction due to loop L3 extends from $\sim z = -5$ to $z = +5$ Å.

manuscript in preparation) suggest that the diffusion coefficients of water molecules within a pore are reduced by a factor of ~5 relative to that of "bulk" water. This seems to correspond with the difference in calculated and experimental conductances.

One may employ such calculations to estimate an "effective" conductance (G_{EFF}) for different β-barrel models. On the basis of the preceding arguments, $G_{EFF} \approx 0.2G_{MAX}$ appears to be a reasonable approximation. Thus, for the $N = 8$, $S = 8$, 12, and 16 β-barrel models one may estimate that (in 0.5 M KCl) $G_{EFF} = 140$, 240, and 480 pS, respectively. These values may be compared with single channel conductances (under physiological conditions, i.e., ~150 mM K^+) of ~20 pS for delayed rectifier K^+ channels and of ~240 pS for BK K^+ (Ca) channels (Hille, 1992). There has been some debate over whether a β-barrel model is appropriate for K^+ channel pore domains. The values of G_{MAX} calculated from radically simplified β-barrel models agree to within an order of magnitude with observed conductances for K^+ channels. This suggests that $N = 8$ β-barrels may indeed form the structural basis of K^+ and related voltage-gated channels. Of course, specific ion-side chain interactions within K^+ channels are likely to reduce the observed conductance below that expected on the basis of the simple diffusion model used to calculate G_{MAX}.

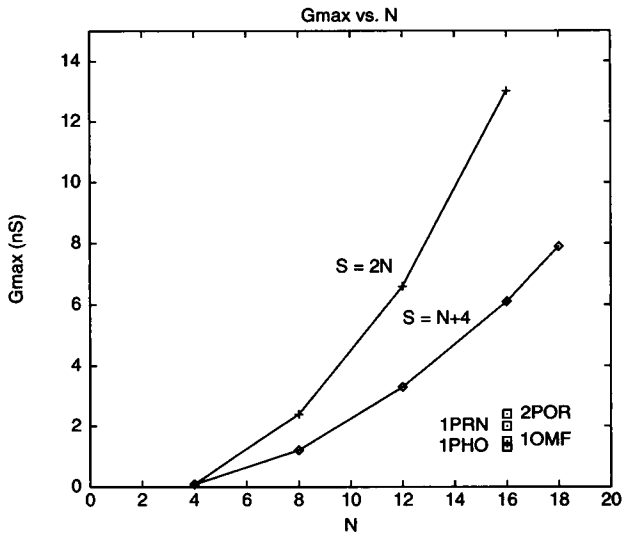

FIGURE 6 G_{MAX} calculations for β-barrel models and for porins, for 0.5 M KCl (ρ = 0.13 Ω). The two curves show G_{MAX} versus N for $S = N + 4$ (◇) and for $S = 2N$ (+). The values for G_{MAX} calculated from the coordinates of the four $N = 16$ porin structures (□) are shown for comparison.

DISCUSSION

Critique of computational methodology

The simulated annealing procedure used in these studies is similar to that already successfully employed in modeling parallel (Kerr et al., 1994; Breed et al., 1995) and antiparallel (Sansom et al., 1995) bundles of TM α-helices, therefore suggesting that it generates physically reasonable models. There is less variability within β-barrel ensembles (backbone RMSD ~0.5 Å) than within ensembles of e.g., Ala_{20} α-helix dimers (RMSD ~1.5 Å). This implies that in the case of β-barrels the final models are somewhat more dependent upon input of correct Cαβ templates. The studies of Chou et al. (1990a,b) and of Murzin et al. (1994a,b) provide a sound theoretical basis for the templates employed. In the present context one may view simulated annealing as allowing the refinement of the Cαβ templates defined on theoretical grounds. This approach is similar in spirit to that adopted by Chou et al. (1990a,b) in their studies of $N = 8$ β-barrel models. Of course, this result implies that in modeling membrane proteins of unknown structure, it will be necessary to evaluate models starting with different Cαβ templates, as automatic convergence to the "correct" β-strand geometry is unlikely to occur.

During simulated annealing backbone torsion angle restraints were applied to (ϕ,ψ) values to retain β-strand conformation. These are unlikely to have biased our models unduly, as a broad region of (ϕ,ψ) space was accessible within the restraints and the restraints were relatively soft (C = 4.0 kcal/mol/rad^2). Preliminary studies of "refinement" of β-barrel models by unrestrained MD simulations in the presence of explicit water molecules within the pore (J. Breed, R. Sankararamakrishnan, I. D. Kerr, and M. S. P. Sansom, manuscript in preparation) reveal some changes in backbone torsion angles. However, comparison of mean torsion angles before and after such refinement reveals no significant shift in mean (ϕ,ψ) values. For example, for an $N = 8$, $S = 12$ β-barrel, before refinement $\phi = -105°$ (±20°), $\psi = +119°$ (±22°) (see Table 1), whereas afterward $\phi = -104°$ (±23°), $\psi = +116°$ (±23°). The pronounced right-handed twist of the β-strands is also retained after refinement.

It may be argued that explicit lipid and water molecules should be included in simulations of transbilayer pores. The omission of these is not too serious, as attention is focused on β-barrel structures per se. A lipid bilayer would be expected to stabilize β-barrels by disfavoring breaking of interstrand H-bonds within an apolar environment. Water molecules within the pore would be expected to have an opposite effect. Comparison with the preliminary results of simulations with explicit solvent molecules within the pore (above) suggests that in the current in vacuo studies the two omissions (bilayer and water) do indeed cancel one another out.

The final simplification in the models is the use of Ala_{10} β-strands. This seems reasonable in that these studies have not concentrated upon sequences resulting in β-barrel formation, but have presupposed that a β-barrel is formed. Although generally considered a helix-stabilizing amino acid, Ala is often found as an interior residue in anti-parallel β-barrels, in which it acts to relieve steric conflicts between larger side chains (Richardson and Richardson, 1989).

Comparison with other modeling studies

It is useful to compare our modeling studies of β-barrels with those of other investigators. A number of studies have been concerned with the conformational properties of isolated β-strands and of β-sheets (e.g., Chothia, 1973; Chou et al., 1982a,b, 1983). More recently, (Chou et al., 1990a,b) modeled idealized $N = 8$ β-barrels formed by Ala_6 and by six residue peptides containing alternating Val and Gly residues. In these studies it was concluded that $S = +8$ barrels were more stable than $S = 0$ or $S = -8$ (i.e., left-handed twist) barrels, and that the source of this stability was primarily intrastrand van der Waals interactions. This is of interest in the context of our finding that van der Waals stabilization of β-barrel models tends to improve as S is increased. In the studies of Chou et al. mean values of $\delta \sim +40°$ were observed, corresponding to a pronounced right-handed twist to the β-strands. This corresponds quite well with our value of $\delta \sim +27°$ for the strands of $N = 8$ barrels. Furthermore, the β-barrel models of Chou et al. (1990a,b) had mean (ϕ,ψ) values of ~(−90°, +115°), which corresponds well with the clustering (for $S > N$) of (ϕ,ψ) about (−90°, +110°) observed for our models (see Fig. 3).

Calculations of G_{MAX} for porins as presented above may be compared with continuum electrostatics calculations

based on the x-ray structures (Karshikoff et al., 1994). Although a detailed consideration of the latter is not appropriate in this context, it is worth noting that both electrostatics calculations and estimations of G_{MAX} suffer from a similar problem, i.e., how to model the continuum properties of solvent within a pore. Both sets of calculations treat pore water in the same manner as bulk water, while admitting that this is an approximation. As discussed above, simulations of the dynamic properties of water molecules within pores offer a possible solution to this difficulty.

Biological relevance

To place our $N = 8$ β-barrel models in a biological context it is useful to consider models of K^+ channels which contain an eight-stranded anti-parallel β-barrel formed by the H5 (sometimes called P) region of the K^+ channel sequence. Three such models have been described in detail. In that of Bogusz et al. (1992) the shear number is $S = 8$. The model of Bradley and Richards (1994) is based on the backbone fold of superoxide dismutase, for which $S = 6$ (Tainer et al., 1982; Chou et al., 1990b). The model of Durell and Guy (1992) contains a right-handed β-barrel with a strand slope angle of $\alpha = 30°$, suggesting again that $S = 8$. In the light of the importance of S in determining the pore properties, K^+ models with values of $S > 8$ may be worthy of further consideration. Preliminary calculations (I. D. Kerr and M. S. P. Sansom, unpublished results) suggest that $S = 12$ models may also be compatible with available data.

Two other models of ion channels that have invoked a central β-barrel, albeit as part of a rather more complex structure. Durell et al. (1994) have suggested a possible model for a channel formed by amyloid β-protein in which two $N = 12$ anti-parallel β-barrels are stacked "head-to-head" to form a bilayer spanning structure. Guy and Durell (1995) have suggested that α/β barrel structures may form the mouths to the pore of the epithelial Na^+ channel. In addition to these ion channel models, β-barrels have also been proposed for the water channel aquaporin (Engel et al., 1994; Fischbarg et al., 1995). Together, these studies reinforce the biological relevance of an understanding of the structural properties of pore formed by β-barrels.

This work was supported by the Wellcome Trust. Our thanks to Dr. Oliver Smart for his program HOLE, and to the Oxford Centre for Molecular Sciences for access to their computational facilities, and to our colleagues (Mr. P. Biggin, Mr. J. Breed, Dr. R. Sankararamakrishnan, and Mr. H. Son) for their comments and interest in this work.

Coordinates for the models described in this paper may be obtained from the following site: http://indigo1.biop.ox.ac.uk/ftp.html.

REFERENCES

Benz, R. 1994. Permeation of hydrophilic solutes through mitochondrial outer membranes: review on mitochondrial porins. *Biochim. Biophys. Acta.* 1197:167–196.

Bogusz, S., A. Boxer, and D. D. Busath. 1992. An $^{SS1\text{-}SS2}\beta$-barrel structure for the voltage-activated potassium channel. *Protein Eng.* 5:285–293.

Bradley, J. C., and W. G. Richards. 1994. Potassium channels: a computer prediction of structure and selectivity. *Protein Eng.* 7:859–862.

Breed, J., I. D. Kerr, R. Sankararamakrishnan, and M. S. P. Sansom. 1995. Packing interactions of Aib-containing helices: molecular modelling of parallel dimers of simple hydrophobic helices and of alamethicin. *Biopolymers.* 35:639–655.

Brooks, B. R., R. E. Bruccoleri, B. D. Olafson, D. J. States, S. Swaminathan, and M. Karplus. 1983. CHARMM: A program for macromolecular energy, minimisation, and dynamics calculations. *J. Comput. Chem.* 4:187–217.

Brünger, A. T. 1992. X-PLOR Version 3.1. A System for X-Ray Crystallography and NMR. Yale University Press, New Haven, CT.

Chiu, S. W., E. Jakobsson, S. Subramanian, and J. A. McCammon. 1991. Time-correlation analysis of simulated water motion in flexible and rigid gramicidin channels. *Biophys. J.* 60:273–285.

Chiu, S. W., J. A. Novotny, and E. Jakobsson. 1993. The nature of ion and water barrier crossings in a simulated ion channel. *Biophys. J.* 64: 98–109.

Chothia, C. 1973. Conformation of twisted β-pleated sheets in proteins. *J. Mol. Biol.* 75:295–302.

Chothia, C., M. Levitt, and D. Richardson. 1981. Helix to helix packing in proteins. *J. Mol. Biol.* 145:215–250.

Chothia, C., and A. G. Murzin. 1994. New folds for all-β proteins. *Structure.* 1:217–222.

Chou, K. C., L. Carlacci, and G. G. Maggiora. 1990a. Conformational and geometrical properties of idealized β-barrels in proteins. *J. Mol. Biol.* 213:315–326.

Chou, K. C., A. Heckel, G. Nemethy, S. Rumsey, L. Carlacci, and H. A. Scheraga. 1990b. Energetics of the structure and chain tilting of antiparallel β-barrels in proteins. *Proteins Struct. Funct. Genet.* 8:14–22.

Chou, K. C., G. Nemethy, and H. A. Scheraga. 1983. Role of interchain interactions in the stabilization of the right-handed twist of β-sheets. *J. Mol. Biol.* 168:389–407.

Chou, K. C., M. Pottle, G. Nemethy, Y. Ueda, and H. A. Scheraga. 1982a. Origin of the right-handed twist and of the increased stability of antiparallel over parallel sheets. *J. Mol. Biol.* 162:89–112.

Chou, K. C., M. Pottle, G. Nemethy, Y. Ueda, and H. A. Scheraga. 1982b. Structure of β-sheets: origin of the right-handed twist and of the increased stability of antiparallel over parallel sheets. *J. Mol. Biol.* 162: 89–112.

Chou, K. C., and H. A. Scheraga. 1982. Origin of the right-handed twist of β-sheets of poly(L-Val) chains *Proc. Natl. Acad. Sci. Usimulated annealing.* 79:7047–7051.

Cowan, S. W., T. Schirmer, G. Rummel, M. Steiert, R. Ghosh, R. A. Pauptit, J. N. Jansonius, and J. P. Rosenbusch. 1992. Crystal structures explain functional properties of two *E. coli* porins. *Nature.* 358:727–733.

Creighton, T. E. 1993. Proteins: Structures and Molecular Properties, 2nd ed. Freeman, New York.

Durell, S. R., and H. R. Guy. 1992. Atomic scale structure and functional models of voltage-gated potassium channels. *Biophys. J.* 62:238–250.

Durell, S. R., H. R. Guy, N. Arispe, E. Rojas, and H. B. Pollard. 1994. Theoretical models of the ion channel structure of amyloid β-protein *Biophys. J.* 67:2137–2145.

Engel, A., T. Walz, and P. Agre. 1994. The aquaporin family of membrane water channels. *Curr. Opin. Struct. Biol.* 4:545–553.

Fischbarg, J., J. Li, M. Cheung, F. Czegledy, P. Iserovich, and K. Kuang. 1995. Predictive evidence for a porin-type β-barrel fold in CHIP28 and other members of the MIP family. *J. Membr. Biol.* 143:177–188.

Fischbarg, J., M. Cheung, F. Czegledy, J. Li, P. Iserovich, K. Kuang, J. Hubbard, M. Garner, O. M. Rosen, D. W. Golde, and J. C. Vera. 1993. Evidence that facilitative glucose transporters may fold as β-barrels. *Proc. Natl. Acad. Sci. Usimulated annealing.* 90:11658–11662.

Fischer, K., A. Weber, S. Brink, B. Arbinger, D. Schunemann, S. Borchert, H. W. Heldt, B. Popp, R. Benz, T. A. Link, C. Eckerson, and U. I. Flugge. 1994. Porins from plants. *J. Biol. Chem.* 269:25274–25760.

Guy, H. R., and S. R. Durell. 1995. Structural model of ion selective regions of epithelial sodium channels. *Biophys. J.* 68: A243.

Hille, B. 1992. Ionic Channels of Excitable Membranes, 2nd ed. Sinauer Associates Inc., Sunderland, MA.

Jap, B. K., and P. J. Walian. 1990. Biophysics of the structure and function of porins. *Q. Rev. Biophys.* 23:367–403.

Jeanteur, D., J. H. Lakey, and F. Pattus. 1991. The bacterial porin superfamily: sequence alignment and structural prediction. *Mol. Microbiol.* 5:2153–2164.

Karshikoff, A., V. Spassov, S. W. Cowan, R. Ladenstein, and T. Schirmer. 1994. Electrostatic properties of two porin channels from *Escherichia coil. J. Mol. Biol.* 240:372–384.

Kerr, I. D., R. Sankararamakrishnan, O. S. Smart, and M. S. P. Sansom. 1994. Parallel helix bundles and ion channels: molecular modeling via simulated annealing and restrained molecular dynamics. *Biophys. J.* 67:1501–1515.

Kraulis, P. J. 1991. MOLSCRIPT: a program to produce both detailed and schematic plots of protein structures. *J. Appl. Crystallogr.* 24:946–950.

Kreusch, A., and G. E. Schulz. 1994. Refined structure of the porin from *Rhodobacter blastica. J. Mol. Biol.* 243:891–905.

Kuyucak, S., and S. H. Chung. 1994. Temperature dependence of conductivity in electrolyte solutions and ionic channels of biological membranes. *Biophys. Chem.* 51:15–24.

Lasters, I., S. J. Wodak, P. Alard, and E. van Cutsem. 1988. Structural principles of parallel β-barrels in proteins. *Proc. Natl. Acad. Sci. Usimulated annealing.* 85:3338–3342.

Murzin, A. G., A. M. Lesk, and C. Chothia. 1994a. Principles determining the structure of β-sheet barrels in proteins. I. A theoretical analysis. *J. Mol. Biol.* 236:1369–1381.

Murzin, A. G., A. M. Lesk, and C. Chothia. 1994b. Principles determining the structure of β-sheet barrels in proteins. II. The observed structures. *J. Mol. Biol.* 236:1382–1400.

Parker, M. W., J. T. Buckley, J. P. M. Postma, A. D. Tucker, K. Leonard, F. Pattus, and D. Tsernoglou. 1994. Structure of the *Aeromonas* toxin proaerolysin in its water soluble and membrane channel states. *Nature.* 367:292–295.

Richardson, J. S., and D. C. Richardson. 1989. Principles and patterns of protein conformation. *In* Prediction of Protein Structure and the Principles of Protein Conformation. G. D. Fasman, editor. Plenum, Press, New York. 1–98.

Sansom, M. S. P., H. S. Son, R. Sankararamakrishnan, I. D. Kerr, and J. Breed. 1995. Seven-helix bundles: molecular modelling via restrained molecular dynamics. *Biophys. J.* 68:1295–1310.

Schirmer, T., T. A. Keller, Y. F. Wang, and J. P. Rosenbusch. 1995. Structural basis for sugar translocation through maltoporin channels at 3.1 A resolution. *Science.* 267:512- 514.

Smart, O. S., J. M. Goodfellow, and B. A. Wallace. 1993. The pore dimensions of gramicidin A. *Biophys. J.* 65:2455–2460.

Tainer, J. A., E. D. Getzoff, K. M. Beem, J. S. Richardson, and D. C. Richardson. 1982. Determination and analysis of the 2 A structure of copper, zinc superoxide dismutase. *J. Mol. Biol.* 160:181–217.

Weiss, M. S., and G. E. Schulz. 1992. Structure of porin refined at 1.8 A resolution. *J. Mol. Biol.* 227:493–509.

White, S. N. 1994. Hydropathy plots and the prediction of membrane protein topology. *In* Membrane Protein Structure: Experimental Approaches. Oxford University Press, New York.

Wilmot, C. M., and J. M. Thornton. 1990. β-Turns and their distortions: a proposed new nomenclature. *Prot. Eng.* 3:479–493.